Editors' Suggestion | Featured in Physics

Dispersionless Coupling among Optical Waveguides By Artificial Gauge Field

Wange Song,[1] Ting Li,[2] Shengjie Wu,[1] Zhizhang Wang,[1] Chen Chen,[1] Yuxin Chen,[1] Chunyu Huang,[1] Kai Qiu,[1] Shining Zhu,[1] Yi Zou,[2] and Tao Li[1,*]

[1]*National Laboratory of Solid State Microstructures, Key Laboratory of Intelligent Optical Sensing and Integration, Jiangsu Key Laboratory of Artificial Functional Materials, College of Engineering and Applied Sciences, Nanjing University, Nanjing 210093, China*

[2]*School of Information Science and Technology, ShanghaiTech University, Shanghai 201210, China*

(Received 19 January 2022; revised 13 February 2022; accepted 14 June 2022; published 26 July 2022)

Coupling among closely packed waveguides is a common optical phenomenon, and plays an important role in optical routing and integration. Unfortunately, this coupling property is usually sensitive to the working wavelength and structure features that hinder the broadband and robust functions. Here, we report a new strategy utilizing an artificial gauge field (AGF) to engineer the *coupling dispersion* and realize a dispersionless coupling among waveguides with periodically bending modulation. The AGF-induced dispersionless coupling is experimentally verified in a silicon waveguide platform, which already has well-established broadband and robust routing functions (directional coupling and splitting), suggesting potential applications in integrated photonics. As examples, we further demonstrate a three-level-cascaded AGF waveguide network to route broadband light to desired ports with an overwhelming advantage over the conventional ones in comparison. Our method provides a new route of coupling dispersion control by AGF and benefits applications that fundamentally rely on waveguide coupling.

DOI: 10.1103/PhysRevLett.129.053901

Light propagating in a waveguide usually has large dispersions determined by the material and guide modes, which have been well studied and many efforts have been made to control these dispersions [1–3]. However, when two or more waveguides are closely arranged, the overlap of guided modes via the evanescent field will lead to the coupling effects [4], which exhibit *coupling dispersion*. In fact, coupling among waveguides is a common effect and plays a key role in the context of integrated photonics [5,6], quantum optics [7,8], optical computing and communications [9–11], etc. However, due to sensitivity of the overlap of guided modes to the wavelength, the coupling exhibits narrow band and highly structure-sensitive characteristics. There have been some attempts to achieve a broadband solution through parameter or structure optimization, e.g., adiabatic and asymmetric structures [12–17], metamaterials [18–22], and topological designs [23]. However, it is still challenging to improve their comprehensive performance to meet the requirement for massive photonic integrations.

As an important physical concept, the artificial gauge field (AGF) allows us to endow photonic systems with a wide range of intriguing phenomena and novel functions, such as an effective magnetic field for photons [24], the photonic Aharonov-Bohm effect [25], and the broadband optical switch [26]. Notably, the AGF induced by curved waveguides exhibits high flexibility for manipulating optical fields, for example, light guiding and negative refraction [27–29], Floquet topological insulators [30–32], and quantum simulations [33–38]. However, most of these works mainly focus on the engineering of photonic band structure and control the light propagation in a global manner. In the viewpoint of comprehensive optical manipulation, the AGF would also provide a powerful tool to enable more precise control of the optical field (e.g., coupling effect), that requires further exploration.

Here, we develop a new coupling dispersion controlling strategy by AGF, and experimentally demonstrate broadband dispersionless and robust coupling in a silicon-on-insulator (SOI) integrated platform. This AGF is introduced by the curved trajectory of waveguides, which gives rise to a flat dispersion of coupling that indicates insensitivity to wavelength and structure variations. We clearly reveal the underlying physics of dispersionless coupling by AGF theory and experimentally verify the behaviors in densely packed silicon waveguides. In addition, three-level cascaded AGF waveguide networks are demonstrated in broadband light routings that show overwhelming advantages over the conventional counterparts. Our work exploits the concept of AGF to control the coupling dispersion and demonstrates the possibility of broadband, robust and dense photonic integrations.

We would like to start from a one-dimensional (1D) coupled waveguide array. In the paraxial approximation, the light propagation is described by the tight-binding coupled mode equation

$$-i\frac{\partial a_j}{\partial z} = c_{j,j-1}a_{j-1} + c_{j,j+1}a_{j+1} + \beta_j a_j, \qquad (1)$$

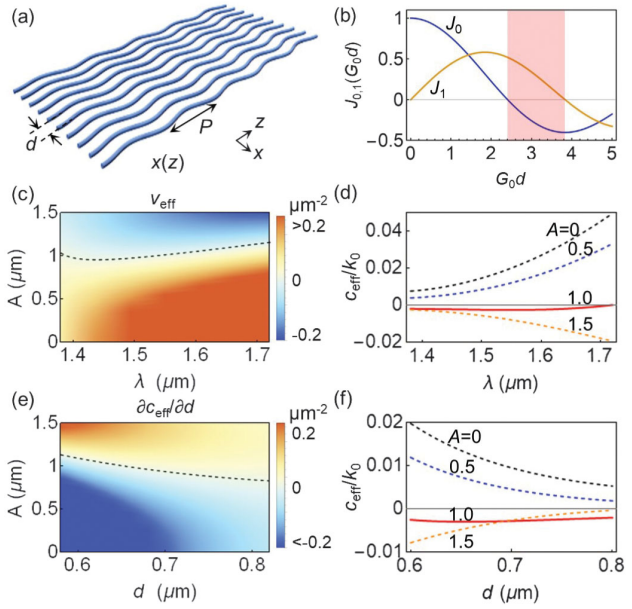

FIG. 1. (a) Schematics of the 1D waveguides with nontrivial trajectories. (b) Zero-(J_0) and first-order (J_1) Bessel modulation of the first kind. There is a sign reversal of J_0 and J_1 in the red region, where the dispersion could be reduced by AGF. (c) The coupling dispersion $\nu_{\rm eff}$ as functions of λ and A with $d = 600$ nm, $P = 10$ μm. The black dashed curve represents $\nu_{\rm eff} = 0$. (d) Effective coupling as a function of λ for different A. From top to bottom, $A = 0$, 0.5, 1.0, and 1.5 μm. (e) $\partial c_{\rm eff}/\partial d$ as a function of d and A with $\lambda = 1550$ nm, $P = 10$ μm. The black dashed curve represents $\partial c_{\rm eff}/\partial d = 0$. (f) Effective coupling as a function of d for different A.

where a_j and β_j is the mode amplitude and propagation constant in the jth waveguide, $c_{j,j+1}$ is the coupling coefficient between the jth and $(j+1)$th waveguides, and $c_{j,j+1} = c^*_{j+1,j}$ (*stands for complex conjugate). For straight waveguides, $c_{j,j+1}$ and β_j are constants along the propagation direction z. However, if waveguides have a bending trajectory following an arbitrary periodic function $x(z) = x(z+P)$, where P is the modulation period [Fig. 1(a)], a nontrivial AGF can be introduced, which modifies $c_{j,j+1}$ to be z dependent (we drop the subscript j, $j+1$ for simplicity) $c'(z) = ce^{iG(z)d}$ [39], where $G(z) = k_0 \partial x/\partial z$ is the curve-introduced AGF, $k_0 = 2\pi n_0/\lambda$ is the wave number in the ambient medium. d is the center-to-center separation between waveguides, and c is the coupling between straight waveguides. In the high-frequency limit ($2\pi/P \gg c$), the z-dependent coupling $c'(z)$ can be averaged to an effective coupling $c'_{\rm eff}$:

$$c'_{\rm eff} = \frac{c}{P}\int_0^P e^{iG(z)d}dz \equiv c_{\rm eff}e^{i\theta}, \tag{2}$$

where $c_{\rm eff} = c\Gamma(G)$ is the coupling strength with $\Gamma(G) = \sqrt{\{(1/P)\int_0^P \cos[G(z)d]dz\}^2 + \{(1/P)\int_0^P \sin[G(z)d]dz\}^2}$ the AGF modulation.

Then, we would like to analyze the dispersion of coupling. Since the coupling phase (θ) will not influence the intensity evolutions of the light, only the dispersion of the coupling strength should be considered. To highlight the wavelength dependence, we express $c_{\rm eff}(\lambda) = c(\lambda)\Gamma[G(\lambda)]$. By calculating the derivative of $c_{\rm eff}$ to λ, the coupling dispersion writes

$$\partial c_{\rm eff}(\lambda)/\partial\lambda \equiv \nu_{\rm eff} = \Gamma[G(\lambda)](\nu_0 + \nu_{\rm AGF}). \tag{3}$$

According to Eq. (3), the effective dispersion $\nu_{\rm eff}$ consists of two terms: the dispersion of straight waveguide coupling [$\nu_0 = \partial c(\lambda)/\partial\lambda$] and the dispersion introduced by the AGF ($\nu_{\rm AGF} = \{c(\lambda)/\Gamma[G(\lambda)]\}\{\partial\Gamma[G(\lambda)]/\partial\lambda\}$). Trivial trajectories (straight or titled waveguides) produce z-independent AGF [$\Gamma(G) \equiv 1$], so that $\nu_{\rm AGF} = 0$. In contrast, for nontrivial trajectories with z-dependent AGF, the emergence of an additional $\nu_{\rm AGF}$ provides an opportunity to compensate for the ν_0 term to realize dispersionless coupling.

As a proof of concept, we consider a common sinusoidal trajectory, i.e., $x(z) = A\sin(2\pi z/P + \varphi)$, where A, P, and φ are the amplitude, period, and initial phase of the trajectory, respectively. The sinusoidal trajectory introduces a well-defined AGF with a simple mathematical form $G(\lambda, z) = G_0(\lambda)\cos(2\pi z/P + \varphi)$, where $G_0(\lambda) = 4\pi^2 A n_0(\lambda)/P\lambda$ is the amplitude of the AGF. Thus, the effective coupling coefficient also has a well-defined form $c_{\rm eff} = cJ_0(G_0 d)$, and the dispersion $\nu_{\rm AGF}$ is reduced to [39]

$$\nu_{\rm AGF} = \frac{cG_0(\lambda)d}{\lambda}\frac{J_1(G_0(\lambda)d)}{J_0(G_0(\lambda)d)}\left(1 - \frac{\partial n_0(\lambda)/\partial\lambda}{n_0(\lambda)/\lambda}\right), \tag{4}$$

where $J_{0(1)}$ is the zero(first)-order Bessel function of the first kind. Interestingly, the coupling dispersion of straight waveguides can be compensated by the AGF as long as J_0 and J_1 have opposite signs. Figure 1(b) shows the J_0 and J_1 functions, and there indeed exists a sign reversal of J_0 and J_1 in the red region. To be mentioned, though there should be other $J_0J_1 < 0$ regions for higher G_0 (corresponding to larger bending amplitude A), the paraxial approximation condition will not be satisfied there, so we will not consider it at present (it will be discussed later). We strictly calculate the $\nu_{\rm eff}$ with respect to λ and A [Fig. 1(c)]. For $A = 0$, $\nu_{\rm eff} > 0$ and increases with λ. As A increases, $\nu_{\rm eff}$ decreases and becomes nearly zero for $A \sim 1$ μm (the black dashed curve represents $\nu_{\rm eff} = 0$), where the dispersion of coupling can be fully compensated by the AGF. Figure 1(d) shows the effective coupling as a function of wavelength for different A. Indeed, the wavelength dispersion of coupling gradually becomes flat as A increases [red curve in Fig. 1(d)], suggesting the insensitivity of the coupling to the wavelength.

To be noted, here the insensitivity to wavelength also indicates robustness against variations in structural

parameters (e.g., waveguide separation d). It can be seen from the derivative of effective coupling c_{eff} to d:

$$\partial c_{\mathrm{eff}}(d)/\partial d = J_0(G_0 d)\partial c(d)/\partial d - J_1(G_0 d)c(d)G_0. \quad (5)$$

Equation (5) reveals that the AGF can also introduce a compensate term to reduce the structural sensitivity to d, as long as J_0 and J_1 have opposite signs [red region in Fig. 1(b)]. Figure 1(e) shows the calculated $\partial c_{\mathrm{eff}}/\partial d$ as functions of d and A. It is found that the $|\partial c_{\mathrm{eff}}/\partial d|$ decreases as A increases and becomes almost zero for $A \sim 1$ μm. Figure 1(f) shows c_{eff} as a function of d for different values of A and the flat curve indeed appears at $A = 1$ μm [red curve in Fig. 1(f)], indicating the insensitivity to waveguide separation.

Then, we would like to verify the theoretical findings on Si-on-insulator (SOI) platform. The designed silicon waveguide is 400 nm wide and 220 nm thick, allowing a fundamental mode at $\lambda = 1550$ nm. The waveguides follow sinusoidal profile with P fixed at 10 μm and A varying from 0 to 1 μm. The waveguide separation d varies from 600 to 750 nm ($\sim\lambda/2$) for dense integration. A commercial finite-element analysis solver (Comsol Multiphysics) is employed for full-wave simulations. It should be mentioned that the theoretical results are derived based on some conditions, including the paraxial approximation, tight-binding approximation, and the high-frequency requirement. According to our setup, we find that the high-density ($d \sim \lambda/2$) integrated system requires a large A/P value for adequate gauge modulation, where the paraxial condition is not satisfied [39]. Consequently, it should lead to deviations from the theory. Figure 2(a) shows the theoretical (black curve) and simulated (red curve) effective coupling as a function of $G_0 d$, which both decrease to zero and then become negative. Differently, the simulation gradually deviates from the theory (Bessel function) as G_0 increases (corresponding to A increases) with an increasing negative discrepancy. Nevertheless, the simulation reveals an identical physics that the effective coupling switches from positive to negative with $G_0 d$ varies. Notably, this enlarged negative discrepancy at the negative coupling regime leads to a stronger coupling strength compared with the theoretical Bessel function, which significantly provides choices of strong coupling strength that give rise to short coupling distance comparable to the straight waveguide cases.

Specifically, Fig. 2(c) shows the simulated coupling coefficient as a function of wavelength for different values of A with $d = 600$ nm. The coupling strength drastically changes by 0.103 $\mu\mathrm{m}^{-1}$ (from 0.036 to 0.139 $\mu\mathrm{m}^{-1}$) over the 1400–1650 nm waveband for straight waveguides (black curve). However, when the AGF is introduced by nonzero A, the change of coupling gradually slows down. In particular, when $A = 0.9$ μm (blue curve), the wavelength dispersion becomes almost flat about -0.046 $\mu\mathrm{m}^{-1}$ with the largest coupling deviations smaller than 0.011 $\mu\mathrm{m}^{-1}$ over

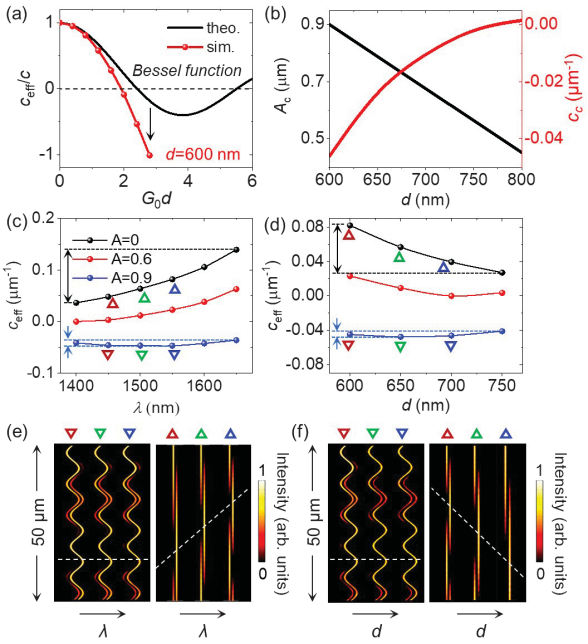

FIG. 2. (a) Theoretical (black curve) and simulated (red curve) effective coupling coefficients as a function of $G_0 d$. Note that in the ideal theoretical case, G_0 should be fixed at a small value to satisfy the paraxial condition and only d varies. In the simulation case, we fix $d = 600$ nm, and $G_0 d$ increases with G_0. (b) Critical bending amplitude A_c (black curve) and corresponding dispersionless coupling c_c (red curve) as a function of waveguide separation d. (c) Simulated c_{eff} as a function of λ for $d = 600$ nm. (d) Simulated c_{eff} as a function of d for $\lambda = 1550$ nm. (e),(f) Simulated optical field dynamics in silicon waveguides without and with AGF for different wavelengths (e) and different waveguide separations (f).

the same waveband, $\sim 1/10$ of the conventional case. Importantly, different values of dispersionless coupling c_{c} can be obtained [Fig. 2(b), red curve] with different critical bending amplitude A_{c} [Fig. 2(b), black curve] by changing the waveguide separation d.

In addition, we also simulate the effective coupling as a function of d to illustrate the insensitivity to structural parameters [Fig. 2(d), $\lambda = 1550$ nm]. It is found that when $A \sim 0.9$ μm (blue curve), the coupling remains stable with the largest deviation <0.0054 $\mu\mathrm{m}^{-1}$ despite a large variation in d (600–750 nm). As a comparison, for straight waveguides (black curve), the coupling undergoes drastic changes of ~ 0.056 $\mu\mathrm{m}^{-1}$ (from 0.082 to 0.026 $\mu\mathrm{m}^{-1}$) for the same variation of d, nearly ten times the case with AGF. For a clearer comparison, we present the simulated propagations of the optical field in the silicon waveguides without ($A = 0$) and with the AGF ($A = 0.9$ μm, $P = 10$ μm, and $\varphi = 0$) [Figs. 2(e) and 2(f)]. The optical field can always couple to another waveguide at a distance (~ 34 μm) for curved waveguides even λ and d change. However, the performance of the traditional waveguides changes drastically.

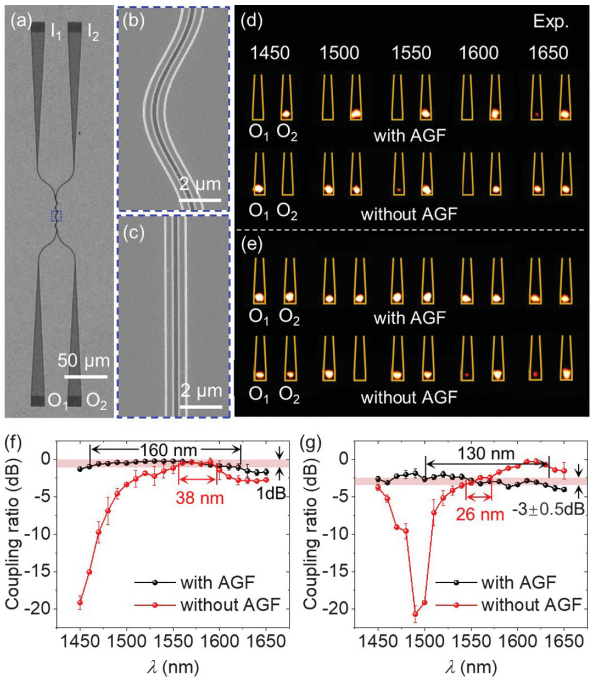

FIG. 3. (a) Microscope image of the samples on a silicon platform. (b),(c) Enlarged scanning electron microscopy images of AGF (b) and conventional (c) samples. (d),(e) Experimentally detected output scattering fields from Port-O_1 and Port-O_2 in AGF and conventional samples with different wavelengths (1450, 1500, 1550, 1600, and 1650 nm) for directional coupling (d) and 50:50 splitting (e) functions. (f) Experimentally measured coupling ratio of Port-O_2 as a function of wavelength for directional coupling, where the 1 dB bandwidth was marked. The error bars represent the deviations of the multiple samples measured. (f) Corresponding results for 50:50 splitting.

To verify our theoretical findings, we experimentally fabricate AGF-based waveguide samples ($A = 0.9$ μm, $P = 10$ μm, $\varphi = 0$, $d = 600$ nm, and 34.5 μm length) [Figs. 3(a), and 3(b)] and conventional straight waveguide samples for comparison [Fig. 3(c)] [39]. A near-infrared laser (1400–1650 nm) is input to Port-I_1 through a single-mode fiber, then the transmission signals of Port-O_1 and Port-O_2 are collected by a multimode fiber and connected to a spectrometer (YOKOGAWA AQ6375) to measure the output intensity (I_{O1} and I_{O2}). A near-infrared camera (Xeva-1.7-320) is used to image the light spots through a microscope objective. To be mentioned, three grating couplers with different periods (700, 800, 900 nm) are used to overcome the bandwidth limitation of the grating coupler [39]. The wavelength-sweep experiments are conducted as individual experiments on different samples with each of these three grating couplers, which only changes the grating efficiencies and seldom changes the ratio data [39].

The experimentally measured output images for different wavelengths (1450, 1500, 1550, 1600, and 1650 nm) are shown in Fig. 3(d), and the coupling ratio data $[I_{O2}/(I_{O2} + I_{O1})]$ are shown in Fig. 3(f). The light input from Port-I_1 couples to Port-O_2 for AGF samples over the 160 nm band with the largest deviation <1 dB (~200 nm band in the simulation), and there is low insertion loss (0.4–0.6 dB, reference to a straight single waveguide of the same length) [39]. However, the 1 dB bandwidth for the conventional sample is 38 nm in experiments and 57 nm in simulation. In addition, we also design and fabricate a sample with a 50:50 splitting ratio (17.5 μm length), and the experimental results are shown in Figs. 3(e) and 3(g). The splitting performance is stable with respect to wavelengths for the AGF sample (~130 nm for the ±0.5 dB bandwidth, most of the data points fall into this range). As a comparison, the straight samples only work at the designed 1550 nm and exhibit large wavelength dependence (~26 nm for the ±0.5 dB bandwidth). To be mentioned, more than 50 samples are fabricated and over 36 valid samples are measured in Figs. 3(f) and 3(g). We discard some invalid measurement data from samples having serious structure flaws, such as the waveguide breaking, grating coupler damage, etc. Furthermore, we also fabricate and measure a set of AGF and straight samples with different waveguide separations d. It is shown that ~130 nm variation of d can hardly affect the performance of the AGF samples (deviation <1 dB), while it loses the functions completely even for several ten nanometers deviations for the straight ones [39]. This robustness promises large tolerance to dimensional uncertainties due to the fabrication, thus allowing scaling to large circuits.

To further show the performance of AGF design in integration, we connect the function units to form three-level cascaded networks, as shown in Fig. 4(a). When the light is input from Port-I_1, it is routed to O_8 [Fig. 4(b)] or equally distributed to all ports [Fig. 4(c)] for the AGF directional coupling and splitting networks, respectively, within a large wavelength range (1400–1600 nm). According to experimental data [Figs. 4(f) and 4(g)], the coupling ratios of AGF cascaded samples stay near the preferred values (0 dB for directional coupling and −9 dB for splitting networks) with the largest deviation <6 dB over a bandwidth of nearly 200 nm. For comparison results of straight-waveguide counterparts, the intensities of eight output ports are chaotic as the wavelength changes [Figs. 4(d) and 4(e)]. There is a large discrepancy in the coupling ratio data with wavelengths varying (>21 dB) and they do not perform well even at designed 1550 nm (~3.58–5 dB). These results show the potential of AGF designs in large-scale and dense photonic integration. We provide more information including the comparisons with literature and broadband elimination of crosstalk among dense waveguides by AGF in [39].

In conclusion, we have developed a new strategy to control the coupling dispersion among optical waveguides by artificial gauge field, which is implemented by

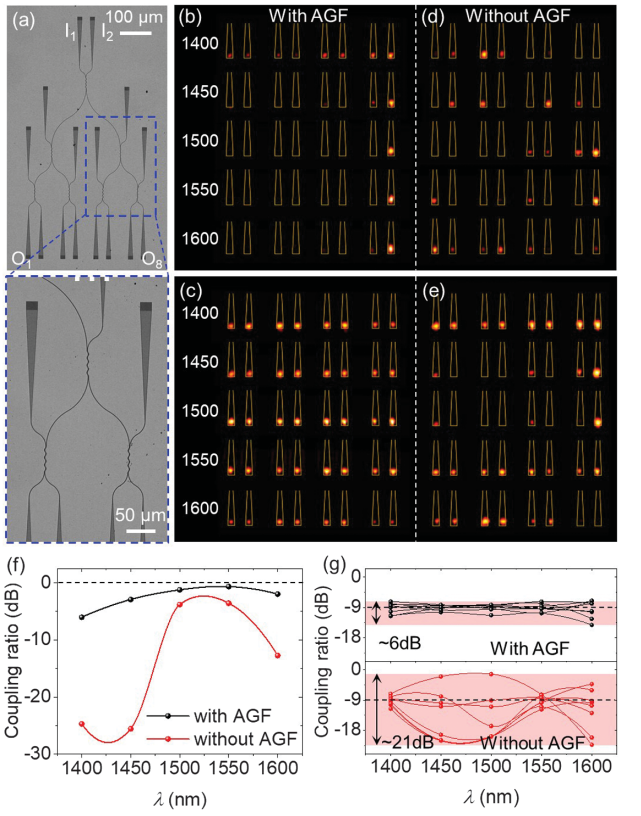

FIG. 4. (a) Microscope images of the three-level cascaded networks. (b),(c) Experimentally detected output scattering fields in AGF directional coupling (b) and 50∶50 splitting (c) cascaded systems for different wavelengths. From top to bottom, $\lambda = 1400$, 1450, 1500, 1550, and 1600 nm. (d),(e) Corresponding results for conventional cases. (f) Coupling ratio for Port-O_8 as a function of wavelengths for cascaded coupling samples. (g) Corresponding results for the cascaded 50∶50 splitting network.

elaborating curved trajectory of waveguides and works out a flat coupling dispersion (dispersionless) in certain broadband. Based on the AGF waveguides, we successfully realize robust directional waveguide coupling and splitting with a bandwidth of 160 nm, whose overwhelming advantages are further experimentally demonstrated in three-cascaded networks as compared with traditional waveguide counterparts. Note that although we start the analysis from the paraxial approximation, it is well proved in later experiments that this condition is not necessary. This work shows the powerful capability of the AGF for dispersion control of waveguide coupling, which opens a new avenue for robust and broadband photonic integrations.

The authors gratefully acknowledge the important contributions of referees to the theoretical derivations in the Supplemental Material. This research was supported by the National Key R&D Program of China (2017YFA0303701) and National Natural Science Foundation of China (No. 12174186, No. 91850204). Tao Li thanks the support from Dengfeng Project B of Nanjing University.

*Corresponding author.
taoli@nju.edu.cn

[1] G. A. Bennett and C. Chen, Wavelength dispersion of optical waveguides, Appl. Opt. **19**, 1990 (1980).
[2] A. C. Turner, C. Manolatou, B. S. Schmidt, M. Lipson, M. A. Foster, J. E. Sharping, and A. L. Gaeta, Tailored anomalous group-velocity dispersion in silicon channel waveguides, Opt. Express **14**, 4357 (2006).
[3] K. Porsezian and K. Senthilnathan, *Guided Wave Optical Components and Devices: Basics, Technology and Applications* (Academic Press, USA, 2006), Chap. 17, p. 251.
[4] A. Yariv, Coupled-mode theory for guided-wave optics, IEEE J. Quantum Electron. **9**, 919 (1973).
[5] S. E. Miller, Integrated optics: An introduction, Bell Syst. Tech. J. **48**, 2059 (1969).
[6] D. Dai, J. Bauters, and J. Bowers, Passive technologies for future large-scale photonic integrated circuits on silicon: Polarization handling, light non-reciprocity and loss reduction, Light **1**, e1 (2012).
[7] A. Politi, M. J. Cryan, J. G. Rarity, S. Yu, and J. L. O'Brien, Silica-on-silicon waveguide quantum circuits, Science **320**, 646 (2008).
[8] M. Zhang, L. Feng, M. Li, Y. Chen, L. Zhang, D. He, G. Guo, G. Guo, X. Ren, and D. Dai, Supercompact Photonic Quantum Logic Gate on a Silicon Chip, Phys. Rev. Lett. **126**, 130501 (2021).
[9] Y. Shen, N. C. Harris, S. Skirlo, M. Prabhu, T. Baehr-Jones, M. Hochberg, X. Sun, S. Zhao, H. Larochelle, D. Englund, and M. Soljačić, Deep learning with coherent nanophotonic circuits, Nat. Photonics **11**, 441 (2017).
[10] M. Tillmann, B. Dakić, R. Heilmann, S. Nolte, A. Szameit, and P. Walther, Experimental boson sampling, Nat. Photonics **7**, 540 (2013).
[11] J. Carolan, C. Harrold, C. Sparrow, E. Martín-López, N. J. Russell, J. W. Silverstone, P. J. Shadbolt, N. Matsuda, M. Oguma, M. Itoh, G. D. Marshall, M. G. Thompson, J. C. F. Matthews, T. Hashimoto, J. L. O'Brien, and A. Laing, Universal linear optics, Science **349**, 711 (2015).
[12] M. Mrejen, H. Suchowski, T. Hatakeyama, C. Wu, L. Feng, K. O'Brien, Y. Wang, and X. Zhang, Adiabatic elimination-based coupling control in densely packed subwavelength waveguides, Nat. Commun. **6**, 7565 (2015).
[13] H. Oukraou, V. Coda, A. A. Rangelov, and G. Montemezzani, Broadband photonic transport between waveguides by adiabatic elimination, Phys. Rev. A **97**, 023811 (2018).
[14] H. Yun, W. Shi, Y. Wang, L. Chrostowski, and N. A. Jaeger, 2×2 adiabatic 3-dB coupler on silicon-on-insulator rib waveguides, In *Proceedings of the Photonics North 2013, 89150V–89150V* (International Society for Optics and Photonics, Ottawa, Canada, 2013).
[15] Z. Lu, H. Yun, Y. Wang, Z. Chen, F. Zhang, N. A. F. Jaeger, and L. Chrostowski. Broadband silicon photonic directional coupler using asymmetric-waveguide based phase control, Opt. Express **23**, 3795 (2015).
[16] S. Chen, Y. Shi, S. He, and D. Dai, Low-loss and broadband 2×2 silicon thermo-optic Mach–Zehnder switch with bent directional couplers, Opt. Lett. **41**, 836 (2016).
[17] G. F. R. Chen, J. R. Ong, T. Y. L. Ang, S. T. Lim, C. E. Png, and D. T. H. Tan, Broadband silicon-on-insulator directional

couplers using a combination of straight and curved waveguide sections, Sci. Rep. **7**, 7246 (2017).
[18] Z. Li, M. Kim, C. Wang, Z. Han, S. Shrestha, A. C. Overvig, M. Lu, A. Stein, A. M. Agarwal, M. Lončar, and N. Yu, Controlling propagation and coupling of waveguide modes using phase-gradient metasurfaces, Nat. Nanotechnol. **12**, 675 (2017).
[19] S. Jahani, S. Kim, J. Atkinson, J. C. Wirth, F. Kalhor, A. A. Noman, W. D. Newman, P. Shekhar, K. Han, V. Van, R. G. DeCorby, L. Chrostowski, M. Qi, and Z. Jacob, Controlling evanescent waves using silicon photonic all-dielectric metamaterials for dense integration, Nat. Commun. **9**, 1893 (2018).
[20] P. Cheben, R. Halir, J. H. Schmid, H. A. Atwater, and D. R. Smith, Subwavelength integrated photonics, Nature (London) 2018) 565 ,**560**).
[21] R. Halir, A. Maese-Novo, A. Ortega-Moñux, I. Molina-Fernández, J. G. Wangüemert-Pérez, P. Cheben, D. Xu, J. H. Schmid, and S. Janz, Colorless directional coupler with dispersion engineered sub-wavelength structure, Opt. Express **20**, 13470 (2012).
[22] Y. Wang, Z. Lu, M. Ma, H. Yun, F. Zhang, N. A. F. Jaeger, and L. Chrostowski, Compact broadband directional couplers using subwavelength gratings, IEEE Photonics J. **8**, 1 (2016).
[23] W. Song, W. Sun, C. Chen, Q. Song, S. Xiao, S. Zhu, and T. Li, Robust and broadband optical coupling by topological waveguide arrays, Laser Photonics Rev. **14**, 1900193 (2020).
[24] K. Fang, Z. Yu, and S. Fan, Realizing effective magnetic field for photons by controlling the phase of dynamic modulation, Nat. Photonics **6**, 782 (2012).
[25] K. Fang, Z. Yu, and S. Fan, Photonic Aharonov-Bohm Effect Based on Dynamic Modulation, Phys. Rev. Lett. **108**, 153901 (2012).
[26] I. A. D. Williamson and S. Fan, Broadband Optical Switch Based on an Achromatic Photonic Gauge Potential in Dynamically Modulated Waveguides, Phys. Rev. Applied **11**, 054035 (2019).
[27] Y. Lumer, M. A. Bandres, M. Heinrich, L. J. Maczewsky, H. Herzig-Sheinfux, A. Szameit, and M. Segev, Light guiding by artificial gauge fields, Nat. Photonics **13**, 339 (2019).
[28] Q. Lin and S. Fan, Light Guiding by Effective Gauge Field for Photons, Phys. Rev. X **4**, 031031 (2014).
[29] Y. Yang, Y. Ge, R. Li, X. Lin, D. Jia, Y.-J. Guan, S.-Q. Yuan, H.-X. Sun, Y. Chong, and B. Zhang, Demonstration of negative refraction induced by synthetic gauge fields, Sci. Adv. **7**, abj2062 (2021).
[30] M. C. Rechtsman, J. M. Zeuner, Y. Plotnik, Y. Lumer, D. Podolsky, F. Dreisow, S. Nolte, M. Segev, and A. Szameit, Photonic Floquet topological insulators, Nature (London) **496**, 196 (2013).
[31] E. Lustig, S. Weimann, Y. Plotnik, Y. Lumer, M. A. Bandres, A. Szameit, and M. Segev, Photonic topological insulator in synthetic dimensions, Nature (London) **567**, 356 (2019).
[32] W. Song, Y. Chen, H. Li, S. Gao, S. Wu, C. Chen, S. Zhu, and T. Li, Gauge-induced Floquet topological states in photonic waveguides, Laser Photonics Rev. **15**, 2000584 (2021).
[33] A. Szameit, Y. V. Kartashov, F. Dreisow, M. Heinrich, T. Pertsch, S. Nolte, A. Tünnermann, V. A. Vysloukh, F. Lederer, and L. Torner, Inhibition of Light Tunneling in Waveguide Arrays, Phys. Rev. Lett. **102**, 153901 (2009).
[34] S. Longhi, M. Marangoni, M. Lobino, R. Ramponi, P. Laporta, E. Cianci, and V. Foglietti, Observation of Dynamic Localization in Periodically Curved Waveguide Arrays, Phys. Rev. Lett. **96**, 243901 (2006).
[35] I. L. Garanovich, A. A. Sukhorukov, and Y. S. Kivshar, Broadband diffraction management and self-collimation of white light in photonic lattices, Phys. Rev. E **74**, 066609 (2006).
[36] A. Szameit, I. L. Garanovich, M. Heinrich, A. A. Sukhorukov, F. Dreisow, T. Pertsch, S. Nolte, A. Tünnermann, and Y. S. Kivshar, Polychromatic dynamic localization in curved photonic lattices, Nat. Phys. **5**, 271 (2009).
[37] J. M. Zeuner, N. K. Efremidis, R. Keil, F. Dreisow, D. N. Christodoulides, A. Tünnermann, S. Nolte, and A. Szameit, Optical Analogues for Massless Dirac Particles and Conical Diffraction in One Dimension, Phys. Rev. Lett. **109**, 023602 (2012).
[38] Y. Plotnik, M. A. Bandres, S. Stützer, Y. Lumer, M. C. Rechtsman, A. Szameit, and M. Segev, Analogue of Rashba pseudo-spin-orbit coupling in photonic lattices by gauge field engineering, Phys. Rev. B **94**, 020301(R) (2016).
[39] See Supplemental Material at http://link.aps.org/supplemental/10.1103/PhysRevLett.129.053901 for more details on the theoretical derivation, numerical simulation, and experiment, which includes Refs. [40–45].
[40] D. H. Dunlap and V. M. Kenkre, Dynamic localization of a charged particle moving under the influence of an electric field, Phys. Rev. B **34**, 3625 (1986).
[41] R. Peierls, Zur Theorie des Diamagnetismus von Leitungselektronen, Z. Phys. **80**, 763 (1933).
[42] J. M. Luttinger, The effect of a magnetic field on electrons in a periodic potential, Phys. Rev. **84**, 814 (1951).
[43] L. Ma, J. Li, Z. Liu, Y. Zhang, N. Zhang, S. Zheng, and C. Lu, Intelligent algorithms: New avenues for designing nanophotonic devices, Chin. Optic. Lett. **19**, 011301 (2021).
[44] F. Zhang, H. Yun, V. Donzella, Z. Lu, Y. Wang, Z. Chen, L. Chrostowski, and N. A. F. Jaeger, Sinusoidal anti-coupling SOI strip waveguides, In *Proceedings of CLEO: Science and Innovations SM1I–7, San Jose, California United States* (Optical Society of America, 2015), 10.1364/CLEO_SI.2015.SM1I.7.
[45] X Yi, H. Zeng, S. Gao, and C. Qiu, Design of an ultra-compact low-crosstalk sinusoidal silicon waveguide array for optical phased array, Opt. Express **28**, 37505 (2020).